Activities on Tropical Ionosphere during 2001-2002

O.L.Colombo(*), M.Hernández-Pajares(**), J.M.Juan(**), J.Sanz(**)

(*) GEST/NASA GSFC Code 926, Greenbelt, Maryland, USA
(**)Research group of Astronomy and Geomatics, gAGE/UPC, Barcelona, Spain

The purpose of this report is to summarize the activities of the authors in the framework of the project studying the Tropical Ionosphere in collaboration with the Polytechnical Hong-Kong University (Ref.# PolyU 5075-01E). It consist on two parts: (1) The capabilities of new algorithms developed by the authors in the parameter domain, in order to provide very precise ionospheric correction in the Tropical ionospheric conditions (Hernández-Pajares, M., J.M. Juan, J. Sanz, O.L. Colombo, Improving the real-time ionospheric determination from GPS sites at Very Long Distances over the Equator, *Journal of Geophysical Research*, 107(A10), 1296, doi:10.1029/2001JA009203, 2002). And (2), the detection of strong Scintillation (observational domain) during the March 2002 campaign in the Tropical Ionosphere, at Hong-Kong and Taiwan.

1. Providing accurate real-time ionospheric corrections from fixed sites at thousands kilometers far

1.1 Introduction

As demonstrated in recent years, it is possible to provide ionospheric corrections from GNSS systems such as the Global Ionospheric Maps computed from GPS data (see for example Wilson et al. 1995). In the case of real-time applications such as wide-area navigation augmentation systems (WAAS, EGNOS..., see for example Hansen et al. 1999) the ionospheric corrections have to be calculated from stations typically separated several hundreds km or more, with only the data gathered until the present epoch. This limitation usually produces worst results than computing the ionospheric corrections in post-process. One way to overcome this natural limitation is to run also, simultaneously, a geodetic program solving the carrier phase biases. Combining both complementary types of information, the ionospheric corrections and also the geodetic outputs can improve significantly. Some examples of that can be found in Hernández-Pajares et al. 2000b for ionospheric corrections, in Colombo et al. 1999 for navigation and in Hernández-Pajares et al. 2001 for real-time tropospheric determination.

The purpose of this paper is to show the synergy between precise ionospheric modeling, with the benefits of a tomographic approach, and precise geodetic computation, in real-time, in still more difficult scenarios: with GPS sites separated by thousands of kilometers, placed in the equatorial region, where the ionospheric electron density presents the strongest values and gradients. At such very long distances, this strategy can help to improve the accuracy in real-time global ionospheric maps, that may be feasible very soon with the shift of the International GPS Service (IGS) towards real-time capabilities (Zumberge et al. 1999). These maps can help to improve the accuracy for single-frequency users.

The paper is organized as follows: In the first part, the technique is described. In the second part of the paper, the study showing the improvement in the availability of the precise ionospheric corrections, is presented in detail. One experiment tested the improvement of real-time ionospheric determinations, using data from GPS permanent stations from one thousand to three thousand kilometers apart. This four-week experiment took place in 2001, under hard ionospheric conditions: in the equatorial region near Solar Maximum, and during the noon TEC seasonal maximum.

1.2 Description of the technique

The free electron ionospheric distribution is approximated by a grid of voxels in which the electron density is assumed constant at a given time in an Earth Centered Inertial (ECI) system (see a typical layout in figure 1). The ionospheric determination is performed solving in real-time, by means of a Kalman Filter (Bierman, 1977), the mean electron density N_e of each illuminated cell i,j,k (in solar longitude, latitude and height respectively), treated as a random walk process, and with typical process noise of 10^9-10^{10} electrons/m^3/$\sqrt{hour}$. The carrier phase data are the only ones used. Then the pseudorange code noise and multipath are avoided. The carrier phase biases B_I (constant in each given continuous arch of carrier phase data for each satellite-receiver pair) are estimated simultaneously as random variables (that become white noise random processes when a cycle-slip happens). In the filter the biases decorrelate in real-time from the electron density values, as far as the satellite geometry changes and the variance of both kind of unknowns became smaller (see equation 1 that represent the model for a given ionospheric datum, between one GNSS satellite and one receiver, being L_1 and L_2 the carrier phases in length units, L_I=L_1–L_2 and N_e the electron density).

$$\begin{aligned} \mathrm{L_I} &= STEC + B_I = \int_{\mathrm{REC}}^{\mathrm{SAT}} N_e dl + B_I = \\ &= \sum_i \sum_j \sum_k (N_e)_{i,j,k} \Delta s_{i,j,k} + B_I \end{aligned} \qquad (1)$$

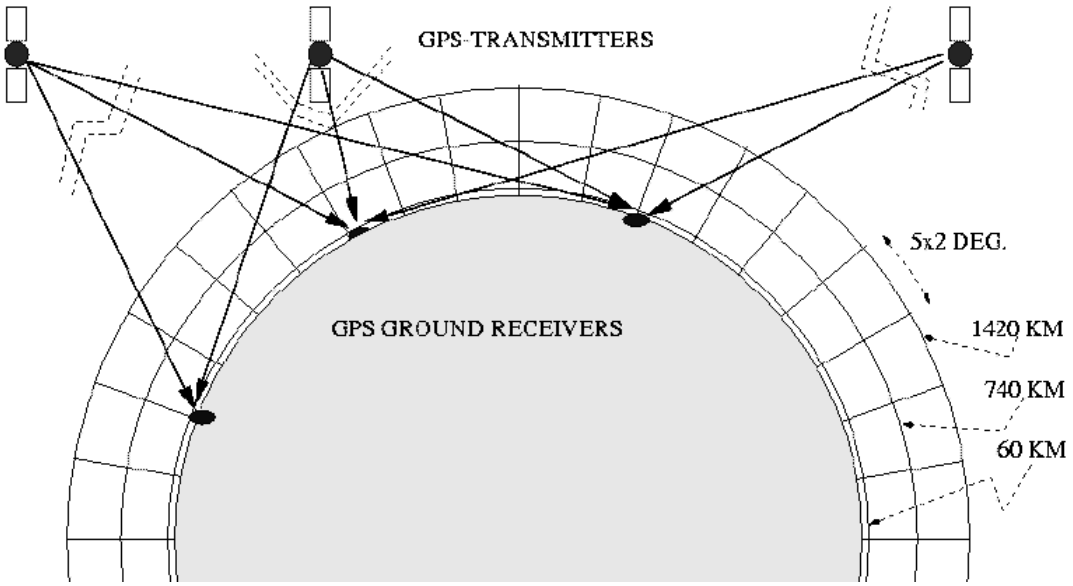

Figure 1: Meridian slice of the voxels in which the ionospheric electron density distribution is decomposed, in the GNSS data driven real-time model, equation 1.

This approach is suitable in particular to detect local features of the electron density distribution, and the use of two layers with ground GNSS data –instead of one as is typically done by many authors– reduces significantly the mismodelling of the electron content determination (Hernández-Pajares et al. 1999a-b)

In the case of Wide Area Differential GNSS (WADGNSS) networks, from these real-time slant total electron content (STEC) corrections obtained by equation 1, it is possible: (see flow chart in figure 2) to form the station-satellite double differences, $\nabla\Delta STEC$, and to obtain a second ambiguity (the widelane) in the reference stations. This and another details of the technique, hereinafter Wide Area Real Time Kinematics (WARTK), referred to the roving receiver can be found for instance in Hernández-Pajares et al. 2000a, 2000b.

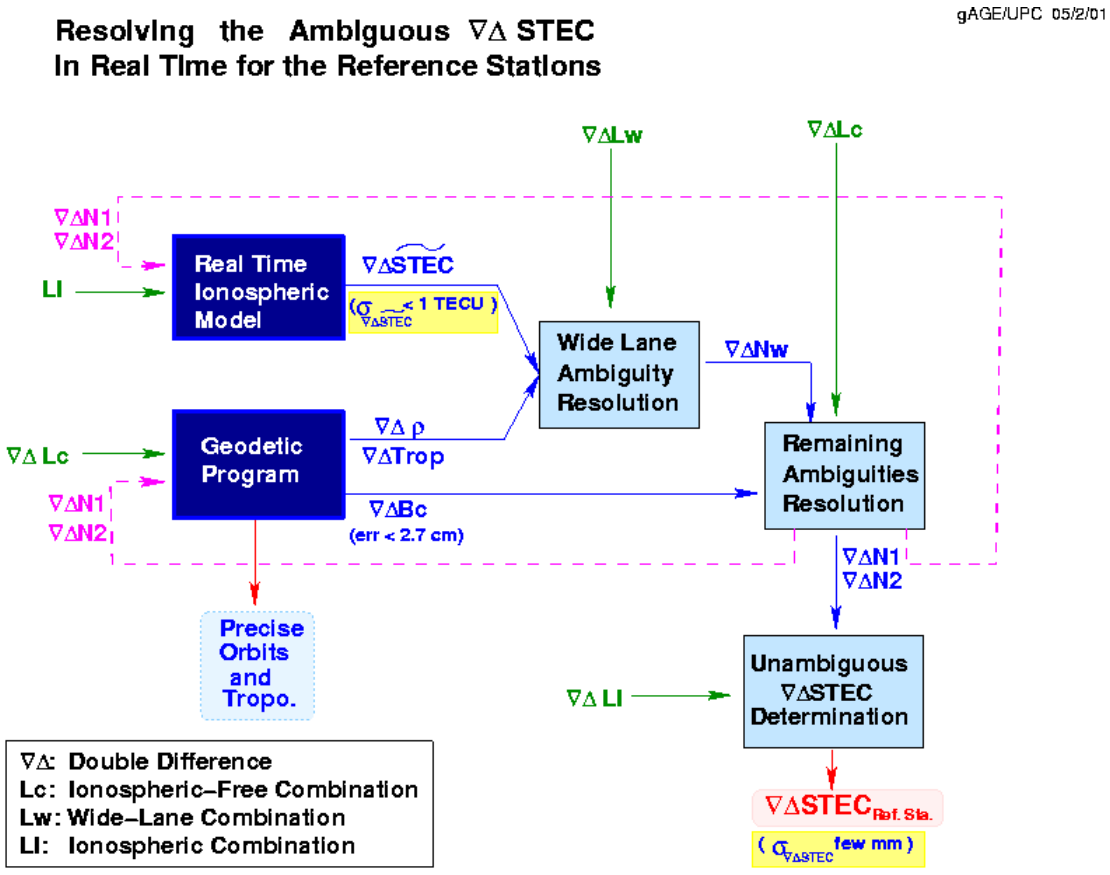

Figure 2: Flow diagram of the main processing steps for the reference stations.

On the other hand, in the case of the reference stations calculation, the long distances and strong electron content gradients can limit the performance of the technique. For this reason, we extend in this paper the algorithm to include the case of permanent/reference stations separated thousands km, using widelane-smoothed code to improve the ionospheric model and hence to help achieve real-time ambiguity determination.

1.3 Experiment and data description

The strategy discussed so far has been used previously only at mid and high latitudes with typical distances of 100-500 km between receivers, and under various ionospheric conditions, giving in all cases good results (see summary in Hernández-Pajares et al. 2001b).

The goal of this new experiment is to assess the performance of the real-time ionospheric model at greater distances, 1000-3000 km, over a wider range of latitudes and over a longer period of time, under some very active ionospheric conditions.

The data corresponds to a set of 12 permanent IGS receivers in Asia and Australia, shown on the map of figure 3. The TOPEX-Poseidon TEC observations are also used as "truth" (see typical footprints in the same figure). It can be seen in the figure that, at these latitudes, this distribution covers both ionospheric equatorial anomalies, and that the distances between sites are in the range of 1000-3000 km.

The data period spans four whole consecutive weeks, from March 6th to April 2nd of 2001, i.e. close to the Solar Maximun, and includes the Spring seasonal maximum of the noon TEC, and several disturbed periods (see Kp index in figure 4).

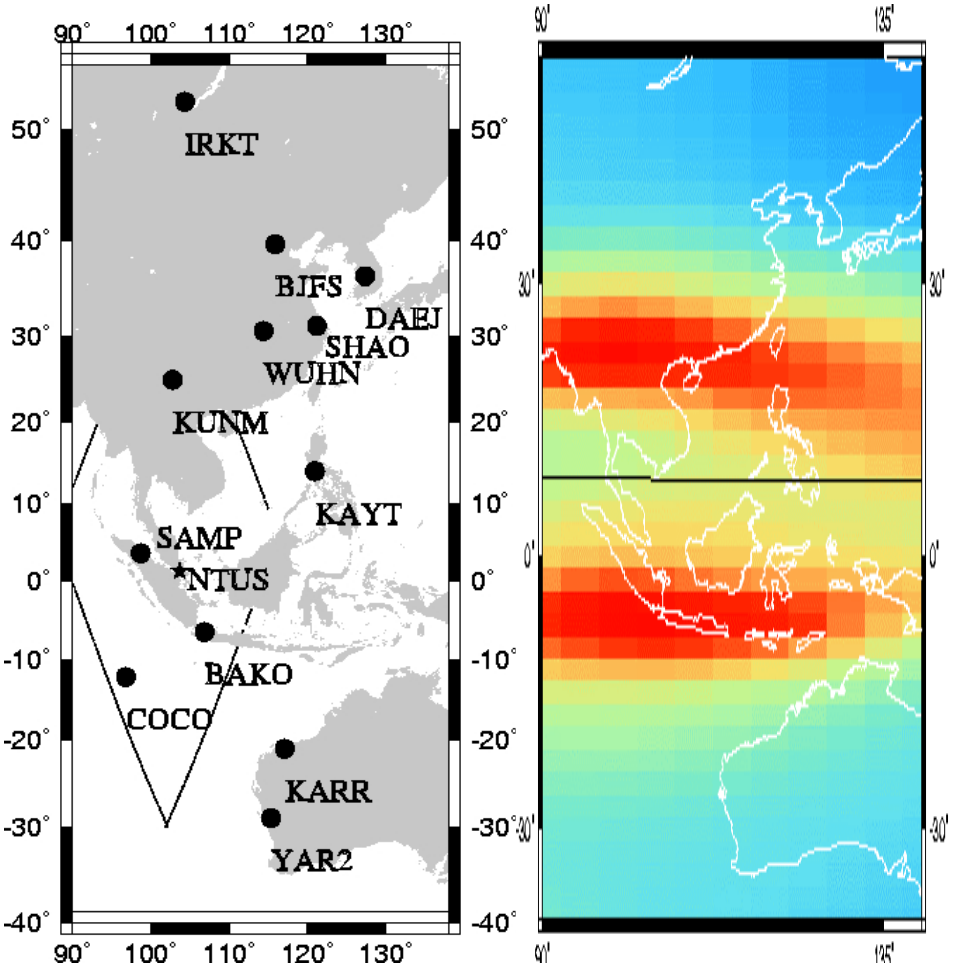

Figure 3: Left plot: IGS stations used in the study of precise ionospheric determination performed during 4 consecutive weeks, between March and April 2001 (the TOPEX tracks compared for the day 67 are also plotted). Right plot: the TEC during the local afternoon (07UT, day 67, March 8th, 2001) and the geomagnetic equator are also represented. The units are tenths of TECU (1 TECU = 10**16 electrons/m**2 ≅ 15 cm in L1). The Appleton north and south tropical anomalies are clearly present, where the TEC reaches values of more than 120 TECU or more, compared to 90 TECU between them, and 60 TECU or less in the north and south edges of the map (source: UPC GIM).

1.4 Computation and Results

In the works mentioned earlier, it has been shown that ambiguity resolution requires the accuracy of the $\nabla\Delta STEC$ correction for the rover to be better than 2 TECU (i.e, a one-sigma precision of 1 TECU). Furthermore, with distances of less than 1000 km between reference stations a success rate higher than 90% can be obtained. This is better by 10% approximately than the rate for the use of the smoothed pseudorange to calculate the wide-lane ambiguity. However, at still greater distances (more than 1000 km) and with high ionospheric variations one can expect a lower percentage. In this case the smoothed code can be useful to help fix the widelane ambiguities, and to slightly constrain the estimation of the real-time ionospheric model.

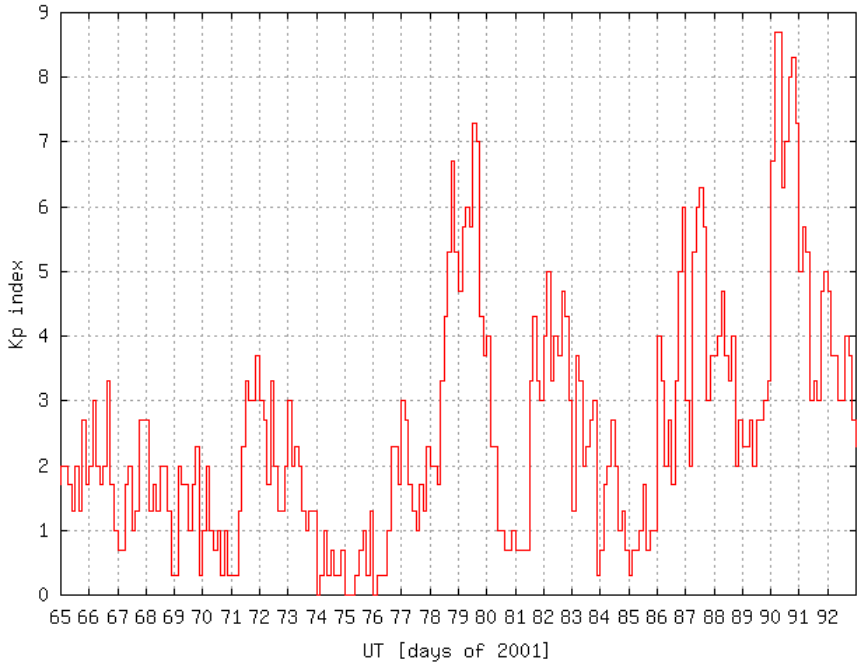

Figure 4: Kp index reflecting the geomagnetic activity for the period of 4 consecutive weeks studied in the second experiment presented in this paper. During the first two weeks aproximately (DOY's 65-77) the geomagnetic activity is low to moderate (Kp <4). However, the last two weeks (DOY's 78-92) the geomagnetic activity attain high and extreme values in certain periods, with 6 < Kp < 9.

The main problem using smoothed code is the presence of multipath, but for permanent receivers it is possible to choose a good antenna location to mitigate this problem. And it is also possible to use the receiver data to estimate the actual antenna multipath pattern in order to correct and strongly diminish the code multipath effect. Only three of the receivers multipath (BJFS, KAYT and SHAO) has been mitigated subtracting a model, obtained from the carrier phase.

The precision of the real-time ionospheric corrections based on carrier phase data from reference stations at very long distances from each other (1000-3000 km) can be assesed in three different ways, for the vertical TEC, the STEC and the $\nabla\Delta STEC$:

First they are compared to the available precise TEC estimates obtained directly from the dual-frequency altimeter on the TOPEX-Poseidon satellite over seas close to the GPS permanent receivers (figure 3).

Two examples of direct comparison of vertical TEC are shown in figure 5, for geomagnetically quiet and very active conditions (days 67 and 90, 2001, with Kp in the ranges 0-3 and 6.5-8.5 respectively, see figure 4). In general the real-time TEC follows the main trends of TOPEX TEC but with higher values, this discrepancy being compatible with the presence of a plasmaspheric electron content of several TECU between the altimeter and the GPS satellites (Lunt et al. 1999). This performance can be still better than the post-processed results, such as distributed UPC Global Ionospheric Maps (GIM) (see Hernández-Pajares et al. 1999a for more details), or any of the available GIM's of other centers (in "IONEX" ionex format, on-line at *ftp://cddisa.gsfc.nasa.gov/pub/gps/products/ionex/YEAR/DOY*). One of the reason for that is the improvement due to fixing the ambiguities in real-time (figure 2). Another difference is the poorest temporal resolution (2 hours) of the distributed GIM's.

A summary of this comparison for the first two weeks of this study, with lower geomagnetic activity, confirms these results. Figure 6 shows the bias and standard deviation of the difference TEC[GPS]-TEC[TOPEX] plotted as a function of latitude, for the two daily TOPEX passes near local noon (top plot) and local midnight (bottom plot), with TOPEX observations relatively close to GPS stations. A typical positive bias of 5TECU, compatible with the plasmaspheric predictions of the authors mentioned above, is observed, with the exception of the interval [-15,-10] degrees in the afternoon sector. In this limited interval, the large bias reaching 10-15 TECU is probably unrealistic. Similar results are obtained for the last two weeks with higher geomagnetic activity.

A second comparison can be made between the observed ambiguous STEC value with its real-time prediction, for a receiver that has not been used in the computations. This is the case for the IGS station NTUS, separated by approximately 600 km from the nearest station, SAMP (see map in figure 3). The variation of STEC can be well predicted, to better than 5 TECU (figure 7).

Finally, in a third study of the performance of this approach the RMS of the error in $\nabla\Delta STEC$ prediction has been calculated using a post-processed solution after fixing as "truth", and then compared to the corresponding success rate in widelane ambiguity resolution (see flowchart in figure 2). It can be seen in figure 8 the results for a baseline of 2354 km (COCO-KARR), and under the influence of the southern Appleton anomaly: the RMS is typically about 1 TECU, and the success rate is greater than the 90% during the four consecutive weeks of the period studied, with a mean rate of 97%. That period includes days of high geomagnetic activity, as shown in figure 4. These results are quite representative, as it can be seen in in table 1, for a set of baselines, for both northern and southern tropical ionosphere.

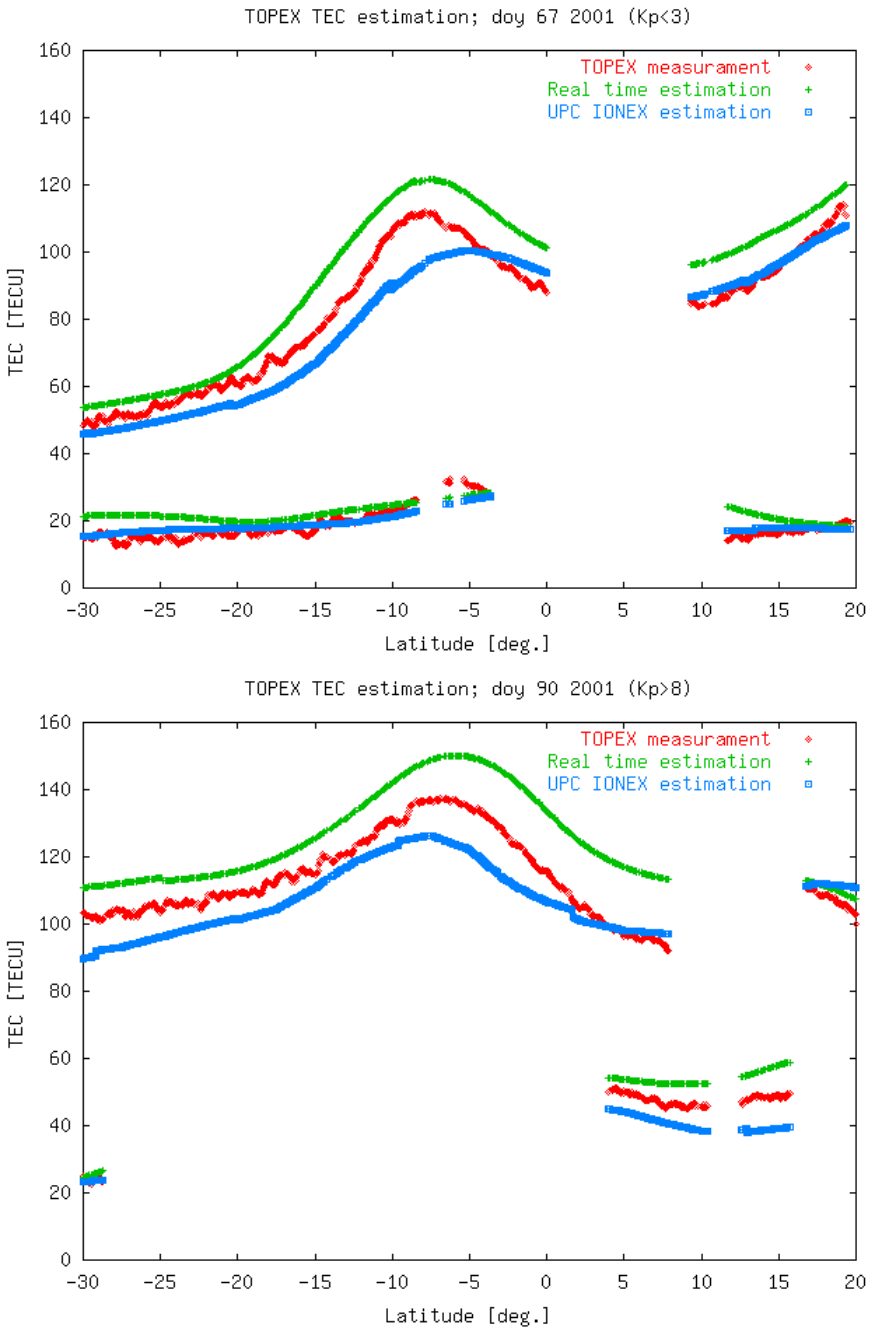

Figure 5: Comparison of real-time ionospheric vertical TEC determination, and post-processed solution, both with GPS data, and TOPEX TEC for a geomagnetically quiet day (March 3rd, 2001, top plot), and a day geomagnetically very disturbed, with Kp ≅ 8 (March 31st, 2001, lower plot).

1.5 Summary and Conclusions

The Wide Area Real Time Kinematic (WARTK) algorithm performs well when used to compute precise real-time ionospheric corrections in WADGPS-like networks. In several experiments previously reported in other publications, the WARTK provided $\nabla\Delta STEC$ better than 2.7 cm (1/4 TECU) for the reference and rover receivers, in middle and high latitudes, and under different ionospheric conditions.

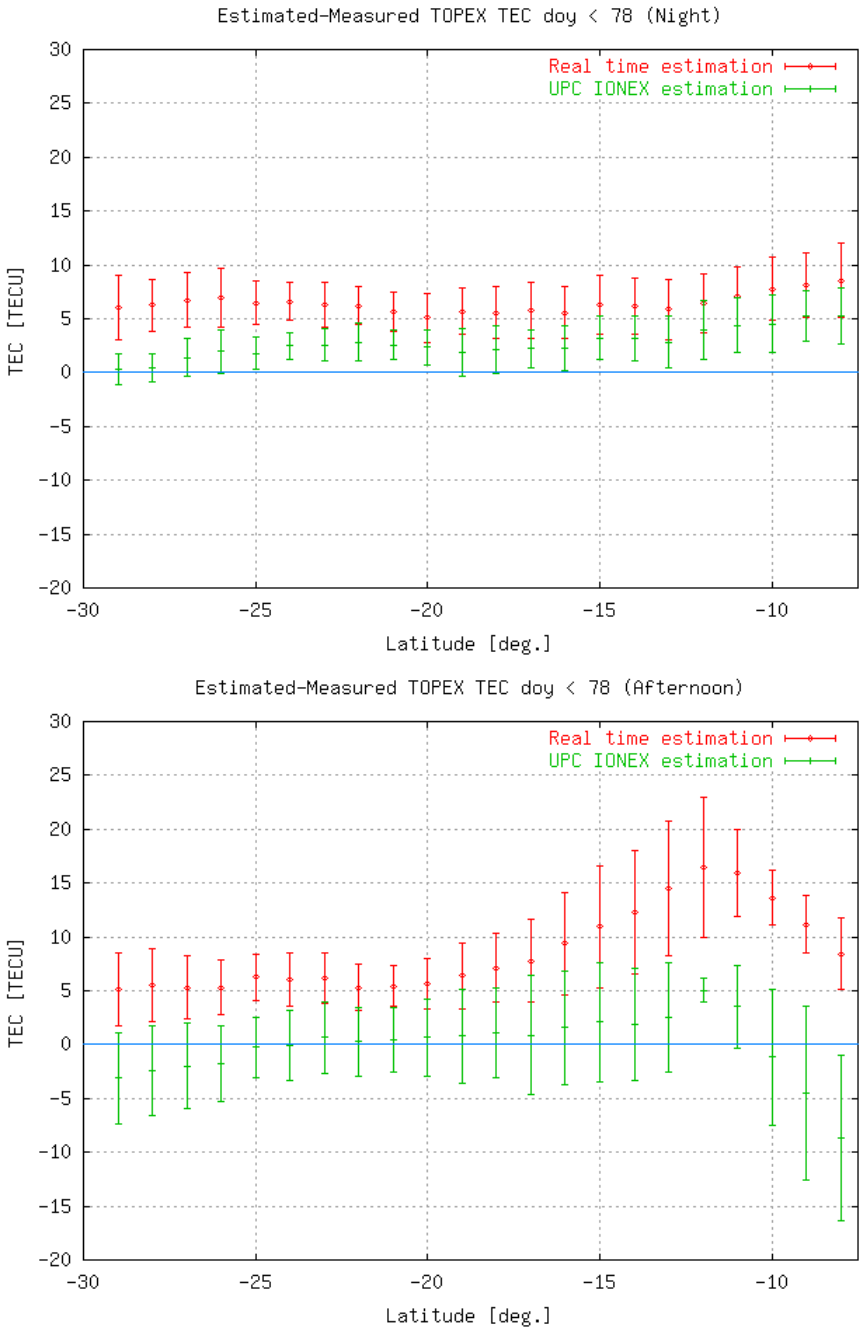

Figure 6: Bias and standard deviation (represented as bar errors) of the differences between GPS TEC and TOPEX TEC for the first part of the studied period with low geomagnetic activity (before DOY 78, March 19th 2001), during the local night (22-04LT) and during the local afternoon (12-18LT). Similar results are obtained with higher geomagnetic activity (starting on DOY 78).

The improvement in real-time STEC determination for the reference GPS stations has been studied in this paper, in one of the worst possible scenarios: very long baselines (1000-3000 km), at low latitudes, and near-Solar Maximum conditions, during four consecutive weeks, including periods of high geomagnetic activity (March-April 2001). The vertical TEC prediction for the TOPEX-Poseidon satellite made with this method was larger than the TEC actually observed with the TOPEX-Poseidon dual frequency altimeter. This discrepancy is compatible with the existence of a significant plasmaspheric electron content between the TOPEX and the GPS satellites. This result is more compatible with TOPEX than the post-processed one at global scale (GIM's), without fixing ambiguities. The standard deviation of the discrepancies with the TOPEX vertical TEC is at the level of 1-3 TECU. This result is compatible with the agreement observed between measured and predicted STEC for GPS receivers not involved in the computations. Finally, in this study the

RMS of the difference between the $\nabla\Delta STEC$ and the post-processed "truth" is about 1 TECU, and the success rate in ambiguity resolution is greater than 90%. Similar results have been achieved for pairs of stations separated by more than 2000 km, and experiencing the strong gradients of the southern equatorial anomaly.

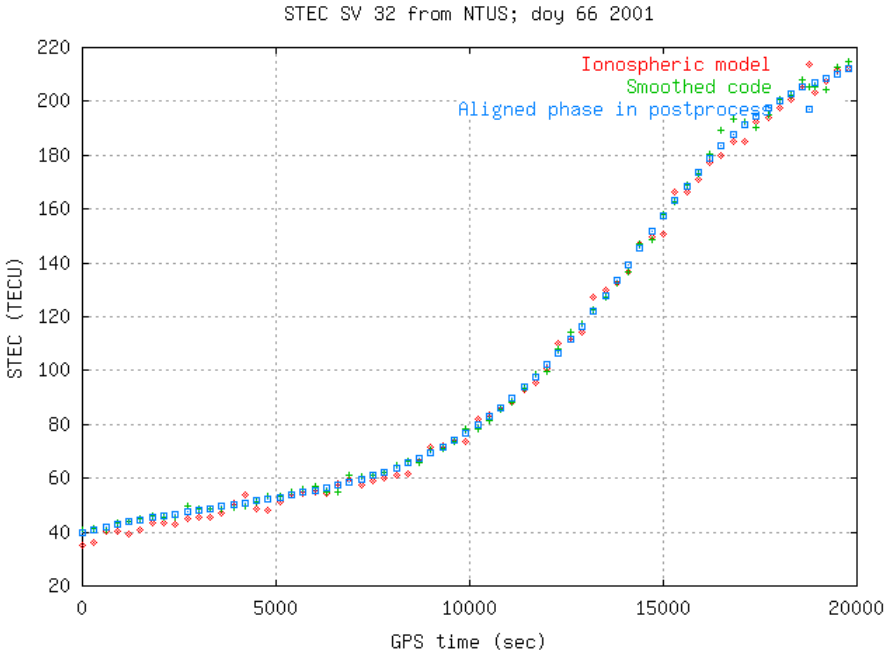

Figure 7: STEC predicted for NTUS, an IGS station not involved in the real-time determination over Asia and Australia, during the day March 7, 2001 (doy 66, March 7th, 2001).

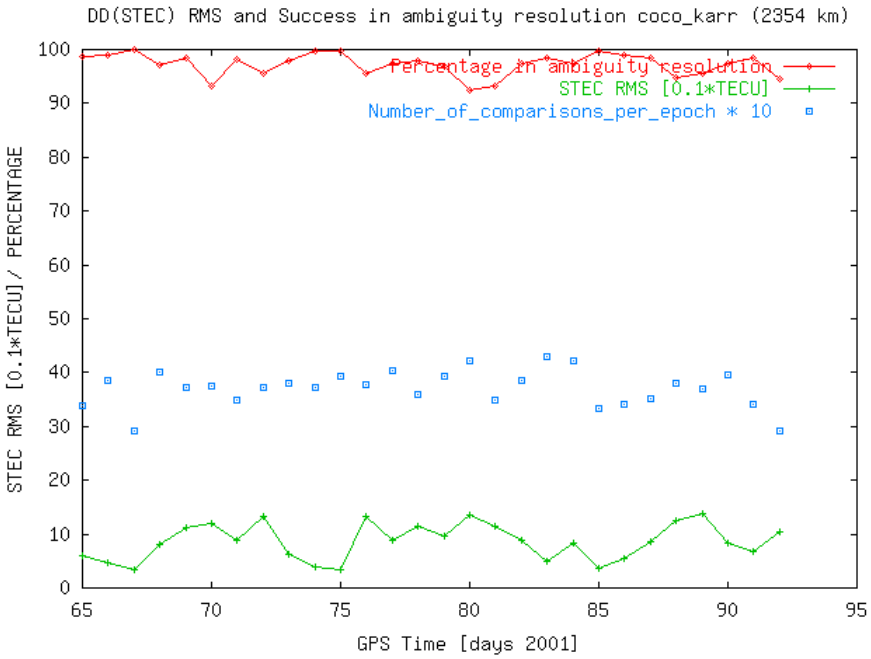

Figure 8: An example of the RMS of the $\nabla\Delta STEC$ real-time determination, and associated success for the double differenced widelane ambiguity, for the baseline from COCO (in the southern Appleton anomaly *footprint*) to KARR in Australia (2354 km away, bottom plot) since 6 March to April 2, 2001. The mean number of observations is also plotted for each day.

Sta.	Ref.	Dist. (km)	% Succ.	RMS [TECU]	# Obs.
IRKT	DAEJ	2507	93	1.2	8329
BJFS	DAEJ	1067	91	1.4	8131
KUNM	DAEJ	2640	95	1.0	3900
WUHN	DAEJ	1369	92	1.4	6358
SAMP	KARR	3341	95	1.1	6441
COCO	KARR	2354	97	0.9	9963
BAKO	KARR	1939	90	1.5	6121
YAR2	KARR	909	97	0.8	12630

Table 1: RMS of the $\nabla\Delta STEC$ real-time determination, and associated success for the double differenced widelane ambiguity, for a set of representative baselines. The distance, in km, and the number of observations are also indicated.

2. Some special features of the GPS observations in the tropical Ionosphere

2.1 Scintillation.

These are fast (seconds-minutes) and rather large fluctuations in the ionosphere, which cause changes in phase and amplitude of the received GPS signals. If severe enough, receivers lose lock, stop racking some satellites, have large errors in measurements, and may stop observing the weaker L2 signal now and then. Noise increases as well. This can be seen when plotting the ion-free combination Lc (L3) as a function of time. Ionospheric scintillation is particularly intense in the tropics, and it seems to be often most intense at the latitudes of HK and Taiwan. It peaks in the hours between sunset and midnight, local time (see attached file with average scintillation map for near-solar maximum conditions).

We observe all of the above in the data from HK and Taiwan. The effect seems more pronounced for the Leicas (2 in Taiwan, 1 in HK) than for the one Trimble (in HK).

We attach a number of small files with plots for the first time-derivative of the ion-free linear combination Lc (or L3), and of the ionospheric observable ("L1-L2"), for all the RINEX files. Numerical time-differencing has been made to eliminate much larger and slower variations in those time series, due to changes in elevation, orbit error, etc, to have a clearer picture of the fast changes, such as scintillation and noise.

Before differencing in time, we have differenced between satellites, to eliminate the effect of the receiver clock error. The reference satellite was the one with the highest elevation, and it was the same for periods of 1 hour or more.

The 14 days of observation were not periods of particularly high ionospheric activity world-wide. The planetary index Kp was mostly <4, one day got to 6, which is "very active", but there is no

correlation that we can see between this index and the fluctuations in the plots, particularly at those times of the evening when scintillation is particularly strong over there.

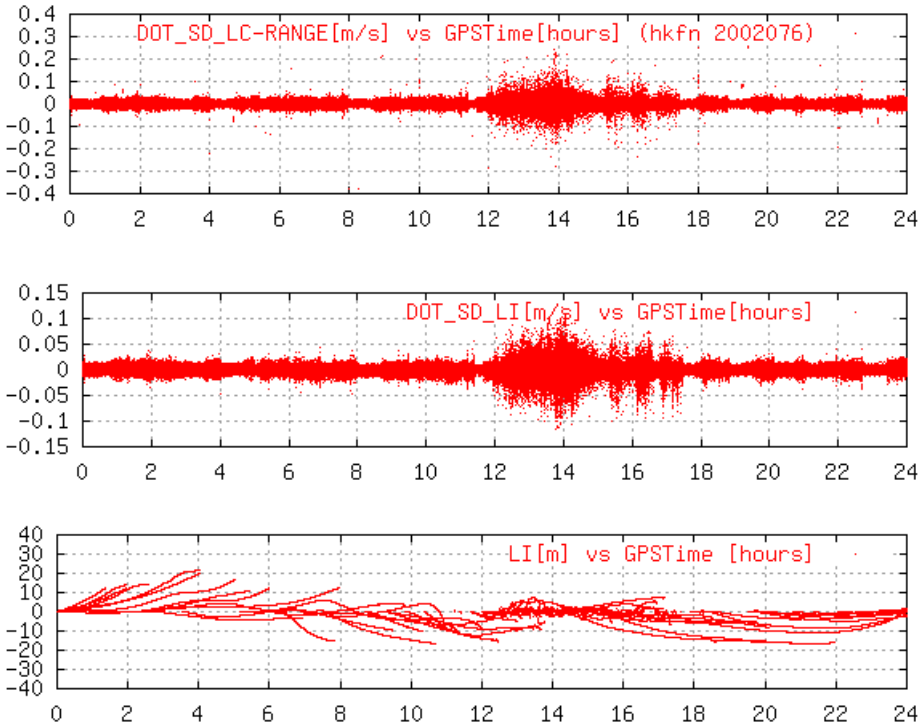

Figure 9: GPS receiver HKFN during day 076, 2002: Derivative of the prefit LC residual (single differences between satellites) at top; derivative of the corresponding ionospheric (geometric free) single differences (center) and plain ionospheric observations (bottom).

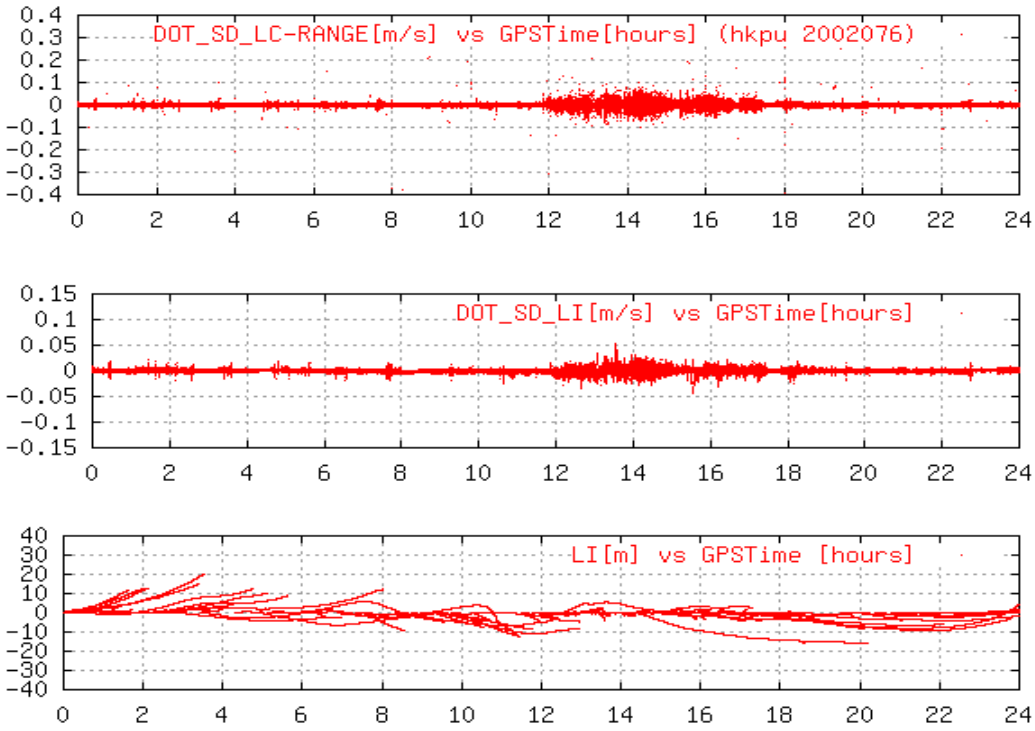

Figure 10: GPS receiver HKPU during day 076, 2002: Derivative of the prefit LC residual (single differences between satellites) at top; derivative of the corresponding ionospheric (geometric free) single differences (center) and plain ionospheric observations (bottom).

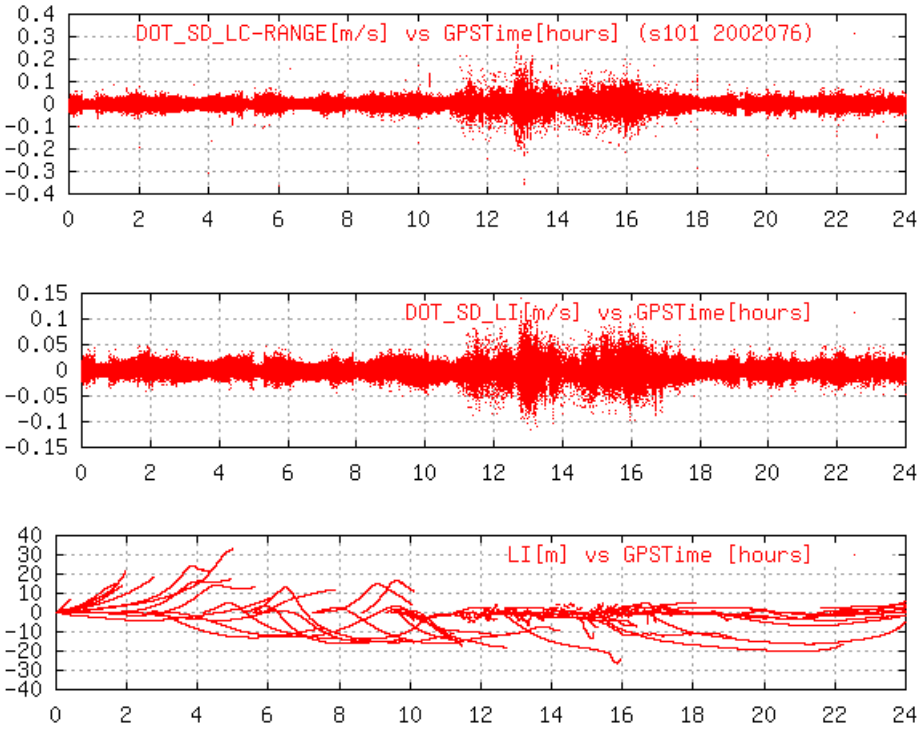

Figure 11: GPS receiver S101 during day 076, 2002: Derivative of the prefit LC residual (single differences between satellites) at top; derivative of the corresponding ionospheric (geometric free) single differences (center) and plain ionospheric observations (bottom).

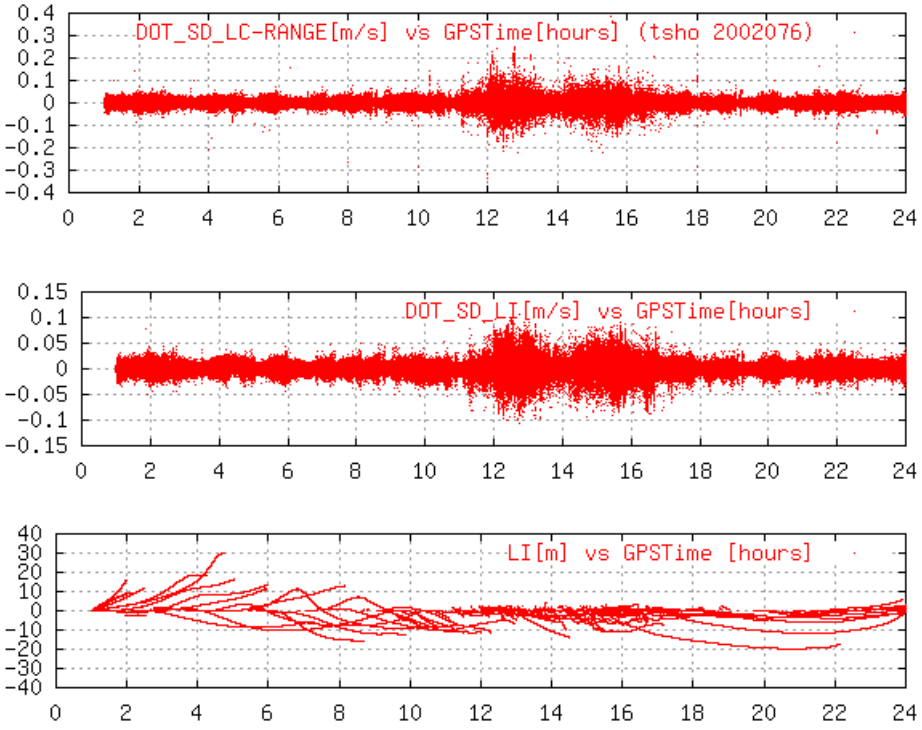

Figure 12: GPS receiver TSHO during day 076, 2002: Derivative of the prefit LC residual (single differences between satellites) at top; derivative of the corresponding ionospheric (geometric free) single differences (center) and plain ionospheric observations (bottom).

Oscar Colombo also attempted to calculate a precise trajectory of one HK receiver with both Taiwan receivers as fiducials. His software's pre-processor threw out many observations, and detected many more cycle-slips than usual (at mid latitudes). In fact, this was so bad in the case of the HK Trimble, that no meaningful solution was possible. In the case of the HK Leica (oddly enough, since the plots show the Leica as noisier, although there were more obs. deleted for the Trimble), the kinematic position could be computed 70% of the time. When they were compared to the static coordinates (adjusted separately in a static solution, relative to the IGS site at Wuhan) the 3-D RMS discrepancy was 12 cm, which is about twice as bad as for the same type of solutions at mid-latitudes, with the same software. The 3-D bias was 20 cm, which is unusually large, and mostly to the East. The static solution, with the same data, differs by > 2 cm from the one computed relative to Wuhan.

These poor results seem to be due mainly to the large number of data edited out. Improving the data-editing algorithms in his software are one of the research interests of Oscar in this joint project, and now that he has all this interesting data, he intends to do that, as time allows, in months to come.

A global view of the ionosphere during these days can be obtained from the UPC ionex files computed daily for IGS. Gif movies available from:

ftp://gage152.upc.es/upc_ionex/2002/DOY_0203DD/upc302DOY.tec0.anim.gif

being DOY the day of year (076-089) and DD the day of the month (17-30, respectively)

2.2 Recommendations

Regardless of how much better the pre-processing algorithms may get, it is clear that scintillation is a serious issue in the tropical region, which is both large and densely populated in many places. So this is a question of great practical importance, and we want to focus on it during this collaboration, as well as looking at other aspects of the ionosphere associated to its disturbed states (traveling disturbance waves, etc.).

It would be interesting to see how other brands of receiver behave under intense scintillation. So it might be a good idea to collect some more data, if that could be arranged, using one of the new Z-surveyor-type from Ashtech, perhaps a new Novatel, etc. Just one of each would be enough.

It may be worth repeating the same experiment 1-2 years from now, Ander intermediate solar cycle conditions, and 3-4 years again, at the time near solar minimum. So we might keep that in mind, even if that is beyond the time of our present collaboration.

REFERENCES

Bierman, G.J., Factorization Methods for Discrete Sequential Estimation, Vol. 128 in Mathematics in Science and Engineering, Academic Press, New York, 1977.

Colombo, O.L., M. Hernández-Pajares, J.M. Juan, J. Sanz and J. Talaya, Resolving carrier-phase ambiguities on-the fly, at more than 100 km from nearest site, with the help of ionospheric tomography, ION GPS'99, Nashville, USA, September 1999.

Colombo O.L., Hernández-Pajares M., Juan J.M. and Sanz J., Ionospheric Tomography Helps Resolve GPS Ambiguities On-the-Fly At Distances of Hundreds of Kilometers During High Geomagnetic Activity, Position Location and Navigation Symposium (PLANS 2000 IEEE conference), San Diego (USA), March 2000.

Hansen A.J., T.F. Walter, P. Enge, Real-time Ionospheric Tomography Using Terrestrial GPS Sensors, Global Positioning System, Selected Papers on Satellite Based Augmentation Systems (SBASs), Vol. VI, The Institute of Navigation, Alexandria, USA, 1999.

Hernández-Pajares M., J.M. Juan and J. Sanz, New approaches in global ionospheric determination using ground GPS data, Journal of Atmospheric and Solar Terrestrial Physics. Vol 61, 1237-1247, 1999a.

Hernández-Pajares M., J.M. Juan, J. Sanz and O.L. Colombo, Precise ionospheric determination and its application to real-time GPS ambiguity resolution, Institute of Navigation ION GPS'99, Nashville, Tennessee, USA, September 1999b.

Hernández-Pajares, M., J.M. Juan, J. Sanz and O.L. Colombo, Application of ionospheric tomography to real-time GPS carrier-phase ambiguities resolution, at scales of 400-1000 km, and with high geomagnetic activity, Geophysical Research Letters, 27, 2009-2012, 2000a.

Hernández-Pajares, M., J.M. Juan, J. Sanz, O. Colombo, H. Van der Marel, Real-time integrated water vapor determination using OTF carrier-phase ambiguity resolution in WADGPS networks, ION GPS'2000, Salt Lake City, September 2000b.

Hernández-Pajares, M., J.M. Juan, J. Sanz, O.L. Colombo, and H. van der Marel, A new strategy for real-time Integrated Water Vapour determination in WADGPS networks, Geophysical Research Letters, 28, 3267-3270, 2001a.

Hernández-Pajares, M., J.M. Juan, J. Sanz, O.L. Colombo, Tomographic modeling of GNSS ionospheric corrections: Assesment and real-time applications, proc. GPS'2001, Salt Lake City, Sept. 2001b

Lunt, N., L.Kersley, G.J. Bailey, The influence of the protonosphere on GPS observations: Model simulations. Radio Science 34, 3, pp.725-732.

Webb, F.H. and J.F.Zumberge, And Introduction to GIPSY/OASIS-II, JPL/CALTECH, JPL D-11088, 1997.

Wessel, P. and Smith, W.H.F, New version of the Generic Mapping Tools released, EOS transactions AGU 76, 326, 1995.

Wilson, B.D. ,A. J. Mannucci,and C. D. Edwards, Subdaily Northern-Hemisphere Maps Using An Extensive Network Of GPS Receivers, Radio Science, 30,3, pp. 639-648, 1995.

Zumberge, J.F., D. Dong, M.R. Marcin and D.A. Stowers, Towards a real-time 1-Hz global GPS network, The International Symposium on GPS GPS99 in Tsukuba, Japan, October 1999.